Study of Urbach tail, bandgap energy and grain-boundary characteristics in CdS by modulated photocurrent spectroscopy

2000 J. Phys.: Condens. Matter 12 4391

(http://iopscience.iop.org/0953-8984/12/19/309)

J. Phys.: Condens. Matter **12** (2000) 4391–4400. Printed in the UK PII: S0953-8984(00)08528-3

Study of Urbach tail, bandgap energy and grain-boundary characteristics in CdS by modulated photocurrent spectroscopy

A E Rakhshani†

Physics Department, Faculty of Science, Kuwait University, PO Box 5969, Safat 13060, Kuwait

E-mail: rakhshani@kuc01.kuniv.edu.kw

Received 8 October 1999

Abstract. Thin cadmium sulfide films were deposited on glass substrates by chemical bath deposition method. The planar photoconductivity was measured as a function of the incident photon energy at different temperatures.

From the fit of experimental results to the existing models, various optoelectronic parameters of CdS, including those related to the temperature dependence of bandgap and the Urbach tail, were evaluated. The measurement technique also helped to evaluate the donor concentration (3×10^{16} cm^{-3}) in the sample used.

In addition to the existing models, the photoconductivity model was extended to account for the effect of incident light in lowering the grain-boundary potential barrier. This allowed the measurement of both, the grain-boundary potential barrier (0.02–0.04 eV) and the energy of the dominant defect level at grain boundaries (0.11–0.13 eV).

1. Introduction

Cadmium sulfide (CdS) is the heterojunction partner of CdTe in thin film solar cells [1]. Among different methods which are being used for the preparation of CdS films, chemical bath deposition (CBD) is the simplest and the most cost-effective technique. The details of deposition by this method have been discussed [2–4]. Despite the fact that bulk CdS has been studied extensively in the past, the structure and the optoelectronic properties of CBD-grown films are not well understood yet. These properties are important since they play major roles in the performance of CdTe/CdS solar cells.

The measurement of photoconductivity at different incident photon energies and at different temperatures provides valuable information on the optoelectronic properties of the material. In this study the theory of ordinary photoconductivity has been extended to account for the effect of the grain-boundary potential barrier. This component can have a substantial contribution to the modulated photoconductivity in polycrystalline films. From the fit of experimental results to this extended model we have determined the activation energy of mobility without the need for mobility measurement. In high resistivity films, mobility measurement is not a convenient task. It has also been shown that several other parameters of the material, including the characteristics of the Urbach tail [5], can be evaluated using modulated photocurrent spectroscopy.

† Fax: (965) 4819374.

0953-8984/00/194391+10$30.00

2. Experimental details

The sample used in this study was grown on a soda-lime glass substrate, at 75 °C, from an alkaline solution consisting of $CdCl_2$ (2 mM), $CS(NH_2)_2$ (3 mM), NH_4OH (640 mM) and NH_4Cl (15 mM). The substrate was placed vertically in the stirred solution for 40 minutes to achieve a film thickness of about 200 nm. Five runs of deposition, each from a fresh solution, were used to obtain a thickness of 1.04 μm. The film thickness was determined from the mass of deposit using a density of 4.82 g cm^{-3} and was also checked against a surface profiler (Tencor, Alfa Step 2000). The sample was annealed in air at 250 °C for 1 h to enhance its photoresponse. Annealing in air increased the dark resistivity of the sample and, hence, reduced the random fluctuations in dark current (Johnson noise), causing an appreciable improvement in the signal-to-noise ratio. The optical bandgap of the film was 2.46 eV at 300 K but it was reduced slightly after annealing. The resistivity of the sample in dark and after annealing was 6×10^5 Ω cm. The average size of grains was 53 nm which was measured from the breadth of the (002) peak of the film x-ray diffraction pattern.

Two parallel stripes of silver paste of 5 mm length and 1 mm separation were deposited on the film surface and were used as the planar contacts. A chopped monochromatic light illuminated the area between the contacts. Photoconductivity measurements were carried out using a PC-controlled set-up consisting of a Sciencetech 9050 grating monochromator, a mechanical chopper set at a frequency of 17 Hz and an Oxford DN 1704 optical cryostat. The wavelength of incident light varied in steps of 2 nm. The photocurrent signal was amplified by a Keithley 428 amplifier, which also supplied 5 V across the contacts. A Stanford Research System (SR530) lock-in amplifier detected the amplified signal. The wavelength dependence of photocurrent was recorded by a PC at different temperatures and was later normalized to the incident photon flux. A calibrated silicon detector determined the spectrum of the incident photon flux.

3. Models

3.1. Photoconductivity

The lateral photoconductivity of thin polycrystalline films detectable between two parallel planar contacts, is due to both, the excess carrier concentration Δn, and the mobility enhancement $\Delta\mu^*$. The latter is due to the reduction of intergrain barrier height. The excess conductivity can, therefore, be written as

$$\Delta\sigma = e\mu^*\Delta n + en\Delta\mu^* \tag{1}$$

where $\mu^* = \mu e^{-\phi_b/kT}$ is the effective mobility, μ and n are the mobility and the concentration of carriers within the grain and ϕ_b is the barrier height at the grain boundary. Equation (1) can be written as

$$\Delta\sigma = e\mu^*\Delta n + \beta e\mu^*\frac{n}{kT}\Psi \tag{2}$$

using $\Delta\mu^* = -\frac{\mu^*}{kT}\Delta\phi_b$ and $-\Delta\phi_b = \beta\Psi$. In the latter relation, the amount by which ϕ_b decreases is taken to be proportional to the incident photon flux Ψ.

In polycrystalline films with a thickness $d \sim 1000$ nm, the carrier diffusion length is much smaller than d and, thus, the excess carrier concentration is given by [6–8]

$$\Delta n = \frac{\Psi\tau(1 - e^{-\alpha d})}{d} \tag{3}$$

where τ is the excess carrier lifetime and α is the absorption coefficient of the incident photons. It should be noted that if d is not much greater than the carrier diffusion length and the surface and bulk recombination velocities are comparable, Δn will contain other terms that make it to go through a maximum as α increases [7]. This results in a peak in the photoconductivity spectrum, a feature that was not observed for the sample examined in this study. In compensated materials the spatially averaged dark carrier concentration, n, is normally temperature dependent. Assuming that n and ϕ_b are controlled by a single grain-boundary defect level with an energy ε_t below the conduction band, Orton *et al* [8] have shown that

$$n = \frac{\eta N N_c G}{N_t - GN} \, \mathrm{e}^{-(\varepsilon_t - \phi_b/kT)} \qquad \text{and} \qquad \phi_b = \frac{eNG^2}{4\varepsilon} \tag{4}$$

where ϕ_b is given in units of eV. The expressions in equation (4) are valid when the grain size, G, is larger than the Debye length $\lambda_D = (\varepsilon kT/Ne^2)^{1/2}$. Here, N is the doping concentration, N_c is the density of states in the conduction band, ε is the material permittivity and N_t ($N_t > NG$) is the surface density of the ε_t defect level at grain boundaries. η is a weak temperature dependent constant given by $\eta = \frac{kT}{\phi_b}(1 - \mathrm{e}^{-\phi_b/kT})$. For a typical value of ϕ_b in the range 0.04–0.1 eV, η is in the range 0.25–0.51 at 300 K. For $N = 3 \times 10^{16}$ cm^{-3} and $\varepsilon = 8.85 \times 10^{-11}$ C^2/N m^2, the Debye length is $\lambda_D = 22$ nm which is less than $G = 53$ nm for this sample and, thus, the condition for the validity of equation (4) is satisfied. The value of $N = 3 \times 10^{16}$ cm^{-3} was obtained from equation (4), using $G = 50$ nm and $\phi_b = 0.03$ eV. The latter is the measurement result which will be discussed. By substituting n from equation (4) and Δn from equation (3) into equation (2) and taking R as the excess conductivity (photoconductivity) normalized to the incident photon flux, it can be shown that

$$R = \frac{e\tau\mu}{d}(1 - \mathrm{e}^{-\alpha d})\,\mathrm{e}^{-\phi_b/kT} + \frac{e\beta\mu}{kT}\,\frac{\eta N N_c G}{N_t - GN}\,\mathrm{e}^{-\varepsilon_t/kT} (G > \lambda_D). \tag{5}$$

The temperature dependence of the pre-exponential factors in equation (5) is mainly due to μ and can be expressed as T^{-n} with $1 < n < 2$. Therefore, a plot of $\ln(RT^n)$ against $1/T$ is expected to yield two slopes from which ε_t and ϕ_b can be evaluated. When $G < \lambda_D$, grains are fully depleted and, as a result, $\phi_b = 0$, $\eta = 1$ and $GN \ll N_t$ [8]. If this condition applies a plot of $\ln(RT^n)$ against $1/T$ yields one slope from which only ε_t is deduced. For above-bandgap photon energies where $E > E_g$, $\alpha d \gg 1$ and R become independent of α and, thus, of E. However, in the range $E < E_g$ where $\alpha d \lesssim 1$, the left term in equation (5), (ordinary photoconductivity) is proportional to α. In this energy range the spectral response R can be used for the measurement of E_g and for the study of the sub-bandgap Urbach tail. The right term in equation (5) represents the modulated photoconductivity which can be observed even in the $E < E_g$ range as long as the incident photons can reduce the value of ϕ_b ($\beta \neq 0$) through sub-bandgap transitions via the grain-boundary states.

3.2. Urbach-Martienssen model

In the energy range $E < E_g$ the optical absorption coefficient normally shows a tail (Urbach tail) which can be expressed by [9–10]

$$\alpha = \alpha_0 \, \mathrm{e}^{(E - E_0)/E_u} \tag{6}$$

where α_0 and E_0 are two constants which can be determined from the converging point of the $\ln(\alpha) - E$ plots measured at different temperatures. E_0 coincides roughly with the energy of the lowest free exciton at zero lattice temperature. The Urbach energy, E_u, is a function of temperature and the structural disorder of the material. The temperature dependence of E_u is

associated with the interaction of electrons/excitons with the optical phonons. Cody's model [11] for E_u is given by

$$E_u = \frac{E_p}{2\sigma_0}\left[X + \coth\left(\frac{E_p}{2kT}\right)\right]. \tag{7}$$

This is an extension to the original model by Urbach [12] and Martienssen [13] in which $X = 0$. Here, X is defined as $X = \langle U_x^2\rangle/\langle U^2\rangle_0$, e.g. the ratio of the mean square deviation of atomic positions caused by structural disorder to $\langle U^2\rangle_0$, the zero-point uncertainty in the atomic positions. E_p is the phonon energy and σ_0 is a parameter that depends on the ionicity of the material [14]. The reported values for σ_0 vary from 0.7 for highly ionic crystals such as NaCl to about 4 for InAs. Its value for CdS is 2.2 [9].

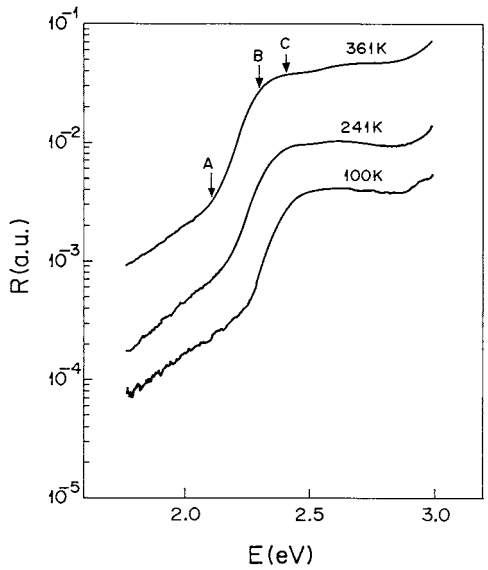

Figure 1. The spectral response of photoconductivity at different temperatures. R is the sample photoconductivity (in arbitrary units) per incident photon of energy E.

The effect of disorder, caused by radiation [15] and by excessive doping [16], on the experimental value of X has been reported. For highly copper-doped CdS films, X can be as large as 32–58 [16].

For single crystals (low X values) of CdS, E_u is 11.9 meV at 300 K and 5.1 meV at 77 K [17]. For a less-defective crystal, these two values are, respectively, 11.0 meV and 2.5 meV [9] and $E_p = 7.5$ meV (a transverse phonon). The optical phonon energies in CdS are 5.5 meV, 28 meV, 29 meV, 31 meV and 38 meV (longitudinal), as determined by Raman spectroscopy [18]. These energies have an average value of 26 meV.

In addition to equation (7), Cody and co-workers [11] have found a linear relationship between E_g and E_u, as expressed by [15]

$$E_g(T, X) = E_g(0, 0) - \langle U^2\rangle_0 D\left[\frac{E_u(T, X)}{E_u(0, 0)} - 1\right] \tag{8}$$

where $E_g(0, 0)$ and $E_u(0, 0)$ are the values of E_g and E_u in a defect free crystal at 0 K and D is the second-order deformation potential which determines the effect of temperature on the bandgap.

4. Results and discussion

The spectral response of the normalized photoconductivity at different temperatures is shown in figure 1. The plots have identical features but are translated along the E-axis due to the temperature dependence of the bandgap and along the R axis due to the temperature dependence expressed by equation (5), as will be discussed. The different regions of the plot obtained at 361 K are marked. For photon energies above point C, R becomes almost flat indicating that in equation (5), $\alpha d \gg 1$. Surface recombination does not apparently play a major role in this sample compared to other CdS samples in which R goes through a peak for $E > E_g$ [7]. In the energy region below point C, R becomes proportional to α. Therefore, a plot of $(RE)^2$ against E in this region should yield a straight line whose intercept with the E axis measures the direct energy bandgap of the material. The range for this linear dependence is limited (e.g. between B and C) due to the presence of the Urbach tail [5] that extends between B and A. At photon energies below point A, a less steep tail is observable. The energy dependence of R in this tail region also has an exponential character. This tail is likely due to the optical transitions between band states and some defect states. The properties of this tail will not be discussed here.

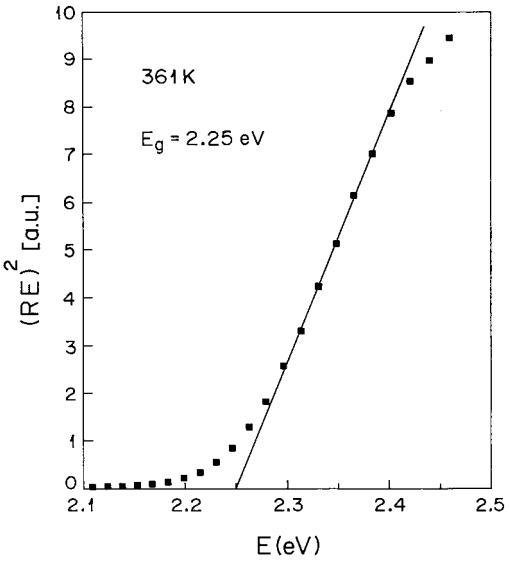

Figure 2. A plot of $(RE)^2$, in arbitrary units, against the incident photon energy E. R is the sample photoconductivity per incident photon. From the horizontal intercept of the line fit, the value of bandgap is obtained 2.25 eV at 361 K.

Figure 2 shows a plot of $(RE)^2$ against E that corresponds to the top plot in figure 1 (361 K). The optoelectrical bandgap determined from the horizontal intercept is 2.25 eV. The result of the bandgap measurement, using this method, at different temperatures is illustrated in figure 3. The variation of E_g with temperature is compared with the Manoogian–Woolley model [19]

$$E_g(T) = E_g(0) - UT^s - V\frac{E_p}{k}\left(\coth\frac{E_p}{2kT} - 1\right). \tag{9}$$

This model includes separately the effect of both lattice dilation and electron phonon interaction. In this equation, $E_g(0)$, U, S, V and E_p are adjustable parameters, nearly

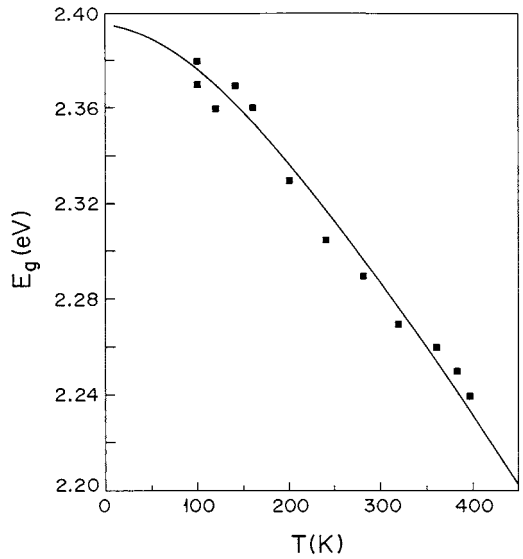

Figure 3. Experimental results on the temperature dependence of the bandgap. The line fit represents the Manoogian–Wooley model [19].

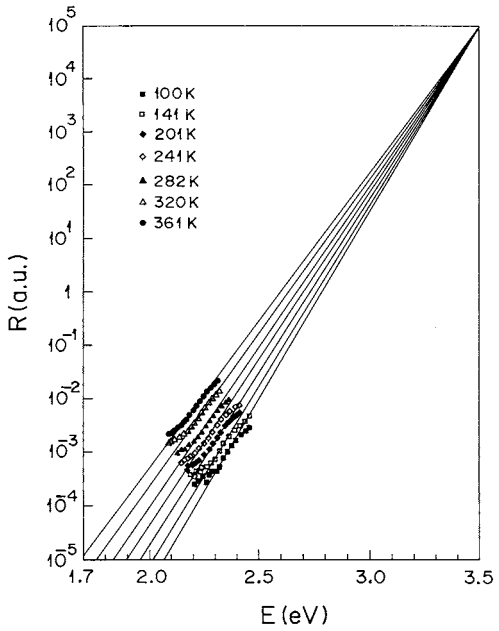

Figure 4. The fit of the measurement results in the Urbach-tail region, where R is proportional to the optical absorption coefficient, to equation (6). The focus-point energy is measured $E_0 = 3.5$ eV.

independent of temperature. E_p is the mean phonon energy that was taken 25 meV. This value was obtained experimentally as will be discussed. Values of $E_g(0)$, U, S and V obtained from the fit of data to equation (9) are, respectively, 2.395 eV, 2.25×10^{-5} eV $K^{-1.42}$, 1.42 and 1.00×10^{-4} eV K^{-1}. Table 1 summarizes these values and the values of other parameters measured in this study. The fit of experimental data to the model is reasonably good as shown

Table 1. Optoelectronic parameters of CdS, obtained by fitting the experimental data to different models express by the quoted equations. N: Donor concentration in grains; ϕ_b: grain-boundary barrier height; ε_t: the energy of the grain-boundary defect level; E_0: Urbach focus energy; E_p: phonon energy; σ_0: a fitting parameter; X: structural disorder parameter; $E_g(0,0)$: energy bandgap at 0 K in a perfect crystal ($X = 0$); $E_u(0,0)$: Urbach energy at 0 K in a perfect crystal ($X = 0$); $\langle U^2\rangle_0 D$: a fitting parameter; $E_g(0)$: energy bandgap at 0 K; U, S, V: fitting parameters.

Parameter	Measured value	Equation used	Reported value	Reference
N	3×10^{16} cm^{-3}	(4)		
ϕ_b	0.02–0.04 eV	(5)	0.03–0.06 eV	[8]
ε_t	0.11–0.13 eV		0.15–0.18 eV	[21]
E_0	3.5 eV	(6)		
E_p	25 meV	(7)	5.5, 28, 29, 31, 38 meV (average 26 meV)	[18]
σ_0	1.19		0.7–4, 2.2	[14, 9]
X	4.82		32–58 (excessively Cu-doped)	[16]
E_g (0,0)	2.86 eV	(8)		
E_u (0,0)	1.8 meV		2.5 meV (E_u at 77 K for single crystal)	[9]
$\langle U^2\rangle_0 D$	14.4 meV			
E_g (0)	2.395 eV	(9)		
U	2.25×10^{-5} eV K$^{-1.42}$			
S	1.42			
V	1.00×10^{-4} eV K^{-1}			
E_p	25 meV			
$\mathrm{d}E_g/\mathrm{d}T$	-0.445 meV K^{-1}		-0.5 meV K^{-1}	[20]

in figure 3. A straight-line fit to the data, however, yields $\mathrm{d}E_g/\mathrm{d}T = -0.445$ meV K^{-1} which is in excellent agreement with the reported value of -0.5 meV K^{-1} [20].

Equation (6) predicts that in the Urbach tail region the straight-line plots of $\ln(\alpha)$ against E for different E_u values (e.g. at different temperatures or at different conditions of structural disorder) should converge to a focus point with coordinates E_0 and α_0. Equation (5) indicates that in the tail region ($\alpha \mathrm{d} \lesssim 1$) R is a linear function of α. Fortunately, both coefficients of this linear function vary weakly with temperature (ϕ_b and ε_t are in the range 0.02–0.13 eV) and therefore, the extrapolated lines of $\ln(R)$ against E are also expected to converge to a focus point. This is shown in figure 4 for several straight-line fits in the temperature range 100–361 K. From figure 4, $E_0 = 3.5$ eV was deduced and also the value of E_u, at different temperatures, was calculated from the slopes of the lines. These values are plotted in figure 5 and are compared with the graphs that are based on equation (7) treating E_p, X and σ_0 as fitting parameters. The best fit, as shown by the solid line, corresponds to $E_p = 25$ meV, $\sigma_0 = 1.19$ and $X = 4.82$. The phonon energy obtained from this fit is almost the same as that (26 meV) corresponding to the average frequencies of phonon excitation determined from Raman spectroscopy, as discussed earlier [18]. $\sigma_0 = 1.19$ and $X = 4.82$ are both in reasonable ranges.

Equation (8) is a linear relationship between the two measurable quantities E_g and E_u. Figure 6 shows the fit of equation (8) to the experimental data points. From this fit the adjustable parameters $E_g(0,0)$, $\langle U^2\rangle_0 D$ and $E_u(0,0)$ were obtained as 2.86 eV, 14.4 meV and 1.8 meV, respectively. $E_u(0,0) = 1.8$ meV is in an acceptable range when compared to $E_u = 2.5$ meV, obtainable from figure 9 of reference [9], for single-crystal CdS at 77 K.

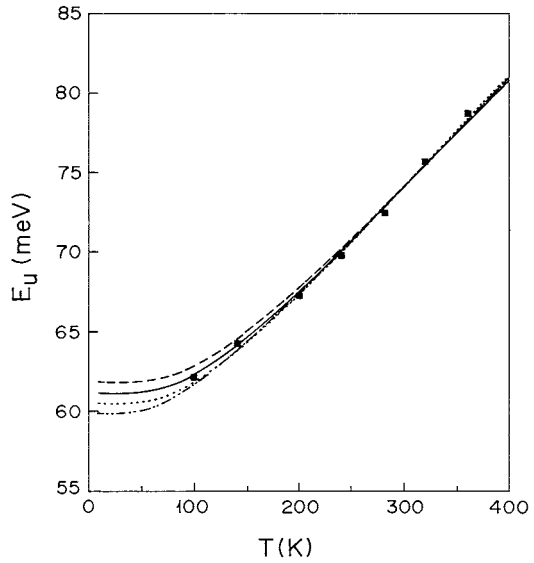

Figure 5. The fit of experimental results to the line plots corresponding to equation (7) with the filling parameters E_p (in meV), σ_0 and X as, respectively, 19.86,1.21,6.3 (——··——), 24,1.16, 4.85 (· · · · · ·), 27, 1.2, 4.5 (– – –) and 25, 1.19, 4.82 (——).

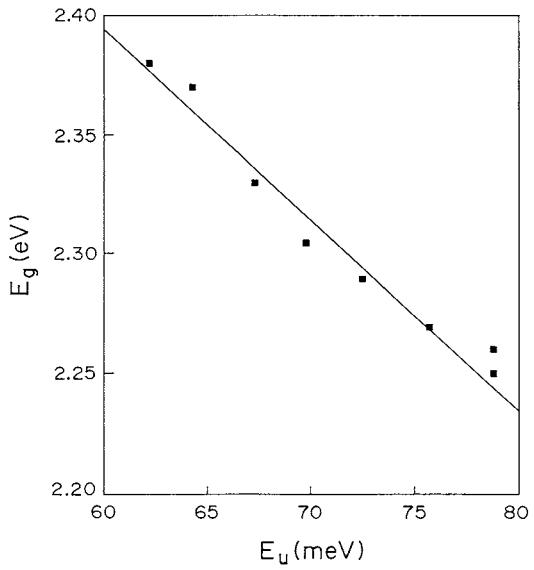

Figure 6. The fit of the measured values of E_g and E_u to equation (8) for fitting parameters $E_g(0, 0) = 2.86$ eV, $E_u(0, 0) = 1.8$ meV and $\langle U^2\rangle_0 D = 14.4$ meV.

Figure 7 shows plots of RT and RT^2 against $1/T$. The R values correspond to the incident photon energy $E = 2.6$ eV, coinciding to the flat region in the R–E plots of figure 1. From the fit of equation (5) to the experimental data ε_t and ϕ_b were measured respectively, 0.11 eV and 0.02 eV, if μ varies with temperature as $\mu \propto T^{-1}$ ($n = 1$) or 0.13 eV and 0.04 eV if $\mu \propto T^{-2}$ ($n = 2$). Due to uncertainty in the temperature dependence of μ, we take ($\varepsilon_t = 0.11$–

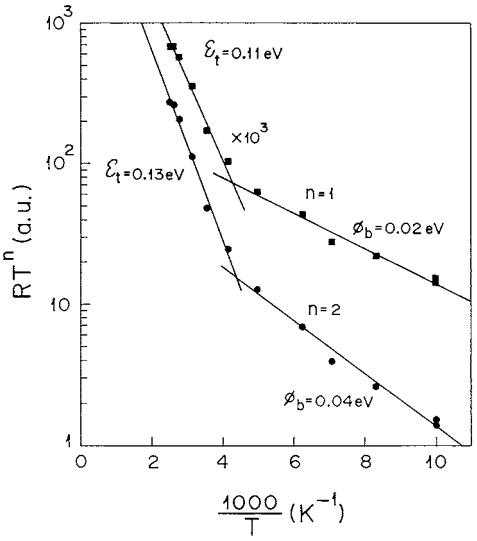

Figure 7. The fit of experimental results to equation (5). The temperature dependence of electron mobility is taken as $\mu \propto T^{-n}$ with $n = 1$ or $n = 2$. In either case the grain-boundary potential barrier ϕ_b and the energy of the grain-boundary defect level ε_t are measured from the slopes of the plots.

0.13 eV and $\phi_b = 0.02$–0.04 eV. These results are in good agreement with $\phi_b = 0.03$–0.06 eV measured from the temperature dependence of mobility in thin CdS films prepared by spray pyrolysis [8]. ϕ_b can have values as high as $\approx$0.15 eV if the average concentration of electrons within the grains is relatively low $\approx 10^{14}$ cm^{-3} [8]. The measured value of $\varepsilon_t = 0.11$–0.13 eV, is in fair agreement with 0.15–0.18 eV obtained from the temperature dependence of dark conductivity in CdS [21]. Taking $\phi_b = 0.03$ eV, $G = 50$ nm (measured value, 53 nm) and $\varepsilon = 8.85 \times 10^{-11}$ C^2/N m^2, the donor concentration is obtained from equation (4) as $N = 3 \times 10^{16}$ cm^{-3}.

5. Conclusions

(1) The extended model of photoconductivity, to account for the effect of the grain-boundary potential barrier, can successfully explain the experimental results in a wide range of temperatures. It enables the measurement of the grain-boundary potential barrier (activation energy of mobility in polycrystalline solids) as well as the energy of the dominant grain-boundary defect level.

(2) Modulated photocurrent spectroscopy provides valuable information on the temperature dependence of the energy bandgap and on the characteristics of the sub-bandgap Urbach-tail.

Acknowledgments

The support from the Research Administration of Kuwait University under project No SP057 is thankfully acknowledged.

References

[1] Chu T L and Chu S S 1994 *Solid-State Electron.* **38** 533
[2] Ortega-Borges R and Lincot D 1993 *J. Electrochem. Soc.* **140** 3464
[3] Oladeji I O and Chow L 1997 *J. Electrochem. Soc.* **144** 2342
[4] Lanning B R and Armstrong J H 1992 *Int. J. Solar Energy* **12** 247
[5] Cody G D 1992 *J. Non-Crystalline Solids* **141** 3
[6] De Vore H B 1956 *Phys. Rev.* **102** 86
[7] Bube R H 1992 *Photoelectric Properties of Semiconductors* (Cambridge: Cambridge University) p 21
[8] Orton J W, Goldsmith B J, Chapman J A and Powel M J 1982 *J. Appl. Phys.* **53** 1602
[9] Kurik M V 1971 *Phys. Status Solidi* a **8** 9
[10] Sumi H and Toyozawa Y 1971 *J. Phys. Soc. Japan* **31** 342
[11] Cody G D, Tiedje T, Abeles B, Brooks B and Goldstein Y 1981 *Phys. Rev. Lett.* **47** 1480
[12] Urbach F 1953 *Phys. Rev.* **92** 1324
[13] Martienssen W 1957 *J. Phys. Chem. Solids* **2** 257
[14] Chichibu S, Mizutani T, Shioda T, Nakanishi H, Deguchi T, Azuhata T, Sota T and Nakamura S 1997 *Appl. Phys. Lett.* **70** 3340
[15] Narayanan K L, Vijaykumar K P, Nair K G M and Thampi N S 1997 *Physica* B **240** 8
[16] Grus M and Sikorska A 1999 *Physica* B **266** 139
[17] Klingshirn C F 1995 *Semiconductor Optics* (Berlin: Springer) p 202
[18] Mitra S S 1969 *Optical Properties of Solids* ed S Nudelman and S S Mitra (New York: Plenum) p 333
[19] Manoogian A and Woolley J C 1984 *Can. J. Phys.* **62** 285
[20] Lynch C T 1989 *Practical Handbook of Material Science* (Boca Raton, FL: Chemical Rubber Company)
[21] Dona J M and Herrero J 1997 *J. Electrochem. Soc.* **144** 4091